Data-Driven Fault Diagnosis of Mooring Systems in Wave Energy Converters

Abishek Subramanian
Dept. of Mechanical EngineeringEngineering Mechanics
Michigan Technological University
Houghton, USA
absubram@mtu.edu

Shangyan Zou
Dept. of Mechanical EngineeringEngineering Mechanics
Michigan Technological University
Houghton, USA
shangyan@mtu.edu

Kai Zhou
The Hong Kong Polytechnic University,
Hong Kong, China
cee-kai.zhou@polyu.edu.hk

Yunsheng Su

Dept. of Mechanical EngineeringEngineering Mechanics
Michigan Technological University
Houghton, USA
ysu2@mtu.edu

Abstract—Ocean renewable energy, particularly wave energy, is experiencing rapid growth in recent years. There is significant interest in moving ocean renewable technologies to offshore regions, given the higher resources (e.g., wave and wind), large area for deployment, less turbulence, and less negative environmental impacts. The mooring systems are the key functional component to guarantee the long-term reliability of floating structures, which, however, are prone to different types of failures. In addition to being consistently exposed to dynamic loads from waves and currents, the mooring lines are also exposed to damages from corrosion, biofouling, and bottom segment displacement. Therefore, it is critical to monitor the condition of the mooring lines' reliability for timely health management and maintenance and to avoid catastrophic failures. This research aims to achieve this objective by developing a new fault diagnosis framework that combines the Autoregressive (AR) model with Convolutional Neural Networks (CNN) to classify fault types and severity under random sea conditions. Two main fault types are considered in this study, including corrosion and biofouling, which are reflected in the numerical model developed for the RM3 Wave Energy Converter (specifically, stiffness decrease and mass increase for the mooring lines). The dynamic responses (surge, heave, pitch motions, and mooring line tensions) generated from this model will be utilized in the proposed fault diagnosis framework, with the AR model extracting features from timedomain data and being used as inputs to CNN for classification. It is noted that this approach not only addresses the challenges posed by random phase shifts in ocean waves but also significantly reduces the computational demand, thereby streamlining the training process and improving the accuracy of fault detection. The simulation results indicate an accurate prediction of the fault type and severity under highly random sea conditions, which demonstrates the feasibility of the proposed method.

Keywords—Wave Energy Converters, Mooring Health Monitoring, Autoregressive model, Convolutional Neural Network,

I. INTRODUCTION

Wave energy stands out among renewable sources for its high-power density and consistent power sources [1]. There has been significant research interest in developing wave energy conversion technologies over the past decades. Various types of Wave Energy Converters (WECs) have been proposed, many of which target deep water applications [2]-[3]. Moreover, offshore deployment of WECs offers

significant benefits, including abundant wave resources, fewer environmental barriers, larger deployment areas, reduced turbulence, and diminished negative environmental and social impacts compared to onshore locations [4]. In this case, ensuring the long-term reliability of WEC mooring systems becomes critical for the stability of the entire system. In a marine environment, mooring lines are subjected to significant dynamic loads from waves and currents. Additionally, these lines experience salt-water corrosion, accumulation of marine organisms, and bottom segment displacement [5]. Failure of these lines could lead to disasters with significant economic, environmental, and social consequences. This is evidenced by more than 30 reported accidents over the past decades [6,7]. Therefore, accurate and reliable monitoring of the operational conditions of mooring lines is critical for the safety of offshore structures. Study [8] provided a comprehensive summary of potential activities for condition control of mooring lines, including annual underwater inspections using ROVs, winch maintenance, periodic changes of fairlead contact, measurement of line diameter, monitoring of structure motions and tension, and non-destructive testing of line segments. While these approaches enhance the safety of permanently installed mooring lines, the cost and risk of human intervention associated with these activities cannot be ignored [9]. Therefore, there is a strong need to develop an automated fault detection framework that can detect and quantify faults in a timely, reliable, and cost-effective manner.

This research aims to address this challenge by developing a novel fault detection framework for WECs capable of accurately and robustly detecting and quantifying different types of faults, considering the randomness of ocean waves. Physically, changes in stiffness and damping are important indicators of the structural integrity of mooring lines, which, in turn, significantly impact the dynamic response of WECs. More specifically, mooring system stiffness may be altered by various factors, including rope creep, damage to the rope structure, seabed trenching, loss of clump weights on the mooring line, and excessive marine growth, among others [10]. Similarly, the damping characteristics of the mooring lines can be significantly influenced by factors like biomass accumulation, which also affects line diameter and mass [11]. To date, despite the existence of model-based approaches to

detect and quantify damage and severity in structures, the application of data-driven machine learning (ML) approaches has been insufficiently studied.

Convolutional Neural Networks (CNNs) are one of the most popular deep learning algorithms, broadly applied in the field of damage detection due to their advanced capabilities in feature extraction and pattern recognition. Traditionally, CNNs have been used to predict structural conditions through image processing. However, image processing-based approaches may not be well-suited for WEC mooring applications given the difficulty and cost of obtaining sampling images. To address this challenge, it has been found that vibration measurement-based signals offer significant damage-related insights into mooring lines. More specifically, the stiffness and damping characteristics of the mooring system shape the time-series dynamic responsessuch as displacement, acceleration of the WEC's floating body, and tensions within the mooring lines—thereby providing distinctive patterns that can be utilized as features for damage detection. This feature has been leveraged by a few recent studies on the damage detection of mooring lines of Floating Offshore Wind Turbines (FOWT). For example, study [12] investigated the fault diagnosis of FOWT mooring lines by applying CNN to time-domain system responses, including motion responses and mooring tensions. A decrease in the mooring stiffness in three different lines is considered in the numerical model to represent the fault. The results demonstrate a good prediction of the fault type and severity. Moreover, study [13] proposed a new fault diagnosis framework by employing both the AR model and CNN to compress the data and enhance damage-sensitive characteristics in the input for CNNs.

AR models are widely applied for creating compact datasets that adeptly localize damage-sensitive data points within larger time-series datasets. This model is particularly effective when the data is assumed to be normally distributed, which holds true for the WEC dynamic responses. Moreover, employing AR coefficients as the CNN inputs effectively mitigates the impact of the random phase shift of irregular ocean waves (superposed by many regular wave components). This is important for fault diagnosis techniques for offshore infrastructures exposed to constantly changing sea conditions. Therefore, in this research, the AR model is adopted in the proposed fault diagnosis framework to extract damage-intensive features and mitigate the impact of constantly changing sea conditions. To further overcome the ocean wave randomness, we propose to incorporate wave characteristics (significant wave height and peak period) in addition to the AR coefficients as inputs to the CNN model to detect and quantify the faults. In addition, the CNN architecture needs to be carefully designed to combine these two types of features effectively. Two types of faults are considered in this research, including corrosion and biofouling (reflected as a decrease in stiffness and an increase in mass in the numerical model). The simulation framework is developed in MATLAB, integrating RM3 WEC hydrodynamics with MoorDyn, which represents the mooring dynamics by applying the lumped mass assumption. Dynamic response data are generated from this simulation framework under varied fault and wave conditions.

The paper is organized as follows. Section II covers the methodology, where we first present the WEC hydrodynamics, AR model, and CNN model, and finally establish the system framework. In Section III, we present and discuss the results, and Section IV draws the conclusion and future work.

II. METHODOLOGY

This section is divided into four subsections to sequentially discuss the methodology. First, we present the WEC hydrodynamic model; then we discuss the AR and CNN models in the second and third sections. In the last section, we present the overall fault diagnosis framework.

A. Numerical model of the WEC and its mooring system
The hydrodynamics of the WEC can be expressed by using the Cummins equation [14].

$$(\mathbf{M}_r + \mathbf{M}_{\infty})\vec{\mathbf{x}} = \vec{F}_e + \vec{F}_{PTO} + \vec{F}_r + \vec{F}_s + \vec{F}_m \tag{1}$$

where $\vec{x} = [x, y, z, \phi, \theta, \psi]$ is the state vector which represents the 6 degrees of freedom (DoF) displacement (surge, sway, heave, roll, pitch, yaw) expressed in the body-fixed frame. The matrix M_r is the rigid body mass and matrix M_{∞} is the added mass at infinite frequency. Moreover, \vec{F}_{PTO} represents the Power Take-Off (PTO) force, \vec{F}_s denotes the linear hydrostatic restoring force, \vec{F}_r represents the radiation force vector [15]. The excitation force \vec{F}_e subject to irregular ocean waves can be computed as the summation of regular wave components as:

$$\vec{F}_e = \Re\{R_f(t) \sum_{i=1}^N \vec{F}_e(\omega_i) \eta(\omega_i) e^{i(\omega_i)t + \phi_i}\}$$
 (2)

where $R_f(t)$ is the ramp function, ω_i and ϕ_i denotes the wave frequency and random phase shift of the ith ocean wave. Moreover, $\eta(\omega)$ denotes the frequency-dependent wave elevation which can be computed from specific wave spectrums and $\vec{\tilde{F}}_{\rho}(\omega_i)$ is the complex excitation force coefficient which can also be obtained from BEM software WAMIT. It is noted that the randomness of the system responses is mainly contributed by the wave excitation force, which is the challenge we are trying to address. \vec{F}_m denotes the mooring force vector which is calculated by MoorDyn in WEC-Sim which applies a lumped-mass based finite element model to model the mooring dynamics [16]. In the lumpedmass formulation, the cable's mass is discretized into point masses located at each node. Here, each node is assigned half the total mass of the two adjacent cable segments. The 3x3 mass matrix for node 'i' can be described as follows:

$$\boldsymbol{m_i} = \frac{\pi}{4} d^2 l \rho l \boldsymbol{I} \tag{3}$$

where I is the identity matrix. The complete equation of motion for each node i is given by:

$$[\mathbf{m}_{i} + \mathbf{a}_{i}]\ddot{\mathbf{r}}_{i} = \mathbf{T}_{i + \left(\frac{1}{2}\right)} - \mathbf{T}_{i - \left(\frac{1}{2}\right)} + \mathbf{C}_{i + \left(\frac{1}{2}\right)} -$$

$$\mathbf{C}_{i - \left(\frac{1}{2}\right)} + \mathbf{W}_{i} + \mathbf{B}_{i} + \mathbf{D}_{pi} + \mathbf{D}_{qi}$$
 (16)

where $\pmb{a_i}$ is the added mass matrix, $\pmb{T}_{i+\left(\frac{1}{2}\right)}$ and $\pmb{T}_{i-\left(\frac{1}{2}\right)}$ is the tension in cable, $\pmb{C}_{i+\left(\frac{1}{2}\right)}$ and $\pmb{C}_{i-\left(\frac{1}{2}\right)}$ are internal damping force in the cable segment $i+\frac{1}{2}$ and $i-\frac{1}{2}$ respectively. \pmb{W}_i is

the net buoyancy at node 'i' and \boldsymbol{B}_i is the force due to interaction between nodes. \boldsymbol{D}_{pi} and \boldsymbol{D}_{qi} are the transverse and tangential drag force. The key parameters of RM3 and the mooring system are presented in Table 1. Fig. 1 illustrates the RM3 with its three mooring lines connected.

Table 1: Key parameters of RM3 WEC and mooring system

When and mooning system
749110
20907301
21306090.66
37085481.11
876420
94419614.57
94407091.24
28542224.82
0.144
126.0
583376000

B. AR Model

The dynamic responses of the WEC and the mooring tensions are then fitted by using the AR model. To prepare the data, the time series signals are normalized as follows:

$$x(t) = \frac{\tilde{x}(t) - \mu}{\hat{\sigma}} \tag{5}$$

where, x(t) is the normalized signal, μ and σ are the mean and standard deviation of the raw signal representing the system's dynamic response. AR model with an order 'p' can be represented as:

$$x(t) = C + \sum_{i=1}^{p} \phi_i x_{t-i} + \varepsilon_t$$
 (6)

where ϕ_i represent the 'p' values of AR coefficients, C is the bias or constant term and ε_t represent Gaussian white noise with a constant arbitrary variance (varies with x(t)). Essentially, the value fitted by the AR model at time 't' is weighted summation of past 'p' time-stamped values along with a bias and Gaussian white noise with a constant arbitrary

variance. This process can be envisioned to be a filtering technique where the white noise is filtered out by the AR coefficients. Broadly, three main processes are involved to effectively perform AR modelling, (1) to find the model order 'p'; (2) to estimate the AR coefficients; (3) to assess the applicability of the model to ensure it is not overfitting and the residuals are not corelated. Residuals can be defined as the error incurred between the actual time-series signals and fitted data by the AR model and can be represented as:

$$\hat{e}(t) = x(t) - \sum_{i=1}^{p} \widehat{\phi}_{i} x_{t-i} - \widehat{C} - \varepsilon_{t}$$
 (7)

where î denote the estimated quantity. In this research, to find the AR modelling order, we assess the convergence of the modified Akaike Information Criterion (AIC) with model order. According to [17], the AIC is defined as:

$$AIC = 2k - ln(\hat{L}) \tag{8a}$$

$$k = 2 * (P + 1)$$
 (8b)

where k represents the number of estimated parameters and $ln(\hat{L})$ represent the maximum value of the log-likelihood function for the fitted AR model. Typically, the random process follows a Gaussian random process and the log-likelihood of a Gaussian random process [18] is defined as:

$$ln(\hat{L}) = \frac{-N}{2} - \frac{-N}{2}ln(\hat{\lambda}) - \frac{N}{2}ln(2\pi)$$
(9a)

$$\hat{\lambda} = \frac{1}{N} \sum \hat{e}(t)^2 \tag{9b}$$

In this equation, N is the number of samples in the time series data. We assume that the residuals $\hat{e}(t)$ are distributed according to independent identical normal distributions (with zero mean). Accordingly, $\hat{\lambda}$ is the variance of the residuals computed using (7). Equation (8a) can be modified and rewritten as:

$$AIC(P) = 2(P+1)/N + ln(\hat{\lambda})$$
(10)

where the constant terms from (8a) are not considered as we are only concerned about the change in AIC values with increasing model order. The first term in (10) penalizes the AIC value with increasing model order while the second term quantifies the model's log-likelihood. It is noted that (10) will represent a converging curve of the AIC. The model order is then determined where the AIC values for all the dynamic response (including motion response and mooring tensions)

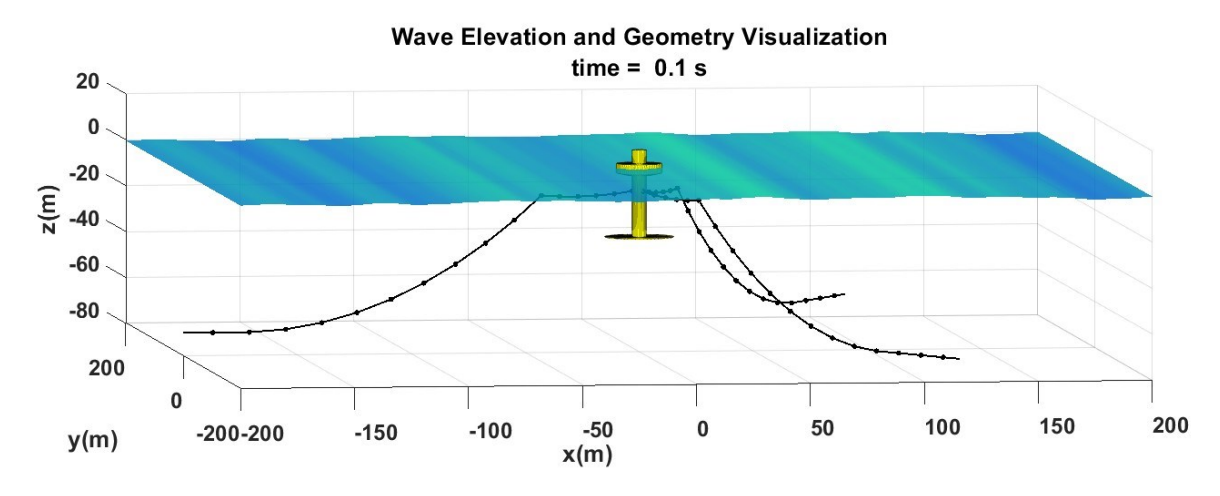


Fig 1: RM3 and its mooring system

converge and stabilize. Once the appropriate model order is found using the AIC plots for all the dynamic responses, the AR coefficients $[\phi_1, \phi_2, \phi_3...\phi_P]$ in (6) is estimated using the Burg method which is also called as method of maximum entropy estimates [19, 20]. The applicability of the derived AR model is then evaluated based on the stationarity of the residuals. Ideally, the residuals should exhibit characteristics of that of a Stationary Gaussian White Noise (SGWN). This can be evaluated by plotting the Auto Correlation Function (ACF) plots for the residual. The residuals can be approximated to be stationary if all the residuals come within 95% confidence bound [21].

C. CNN Model

1D-CNN has been used in this research to extract features from AR coefficients. Fundamentally, 1D-CNN layers excel in processing spatial sequence of data and identify key patterns to distinguish features required for the subsequent layers to process [22]. Mathematically, they convolve the sequence of input data with trained filters (convolution kernels or weights) of pre-defined arbitrary size to extract key features and provide a pathway for the underlying layers of the network to associate the inputs with the target outputs in a supervised learning setup. the convolutional operation of layer l and its output $x_i^{(l+1)}$ is expressed as a sum of convolutional operations across multiple input channels from the previous layer $x^{(l)}$ each with its own set of updated filters or weights $w_{ij}^{(l)}$ which can be represented as:

$$x_i^{(l+1)} = f(\sum_{i=1}^{M^{(l)}} Conv1D(w_{ii}^{(l)}, x_i^{(l)}) + b_i^{(l)})$$
(11)

Where, $x_i^{(l+1)}$ is the output of the i-th feature map at layer (l+1); $w_{ij}^{(l)}$ is the convolution filter that connects the j-th feature map at layer (l) with the i-th feature map at layer (l+1); $x_j^{(l)}$ is the j-th input channel from layer (l); $b_i^{(l)}$ is the bias associated with the i-th feature map at layer (l+1)

1); $M^{(l)}$ is the total number of input channels in layer (l). The function 'f()' is an activation function, such as Rectified Linear Unit (ReLU), sigmoid or tanh applied element wise. The activation function adds a non-linearity to identify relationships between two layers. In our study we have used ReLU activation function which is particularly prominent [23] represented as:

$$f(x) = \max(0, x) \tag{12}$$

1D-CNN plays a pivotal role in extracting key features from signals and mastering complex relationships within the data sequence. Their proficiency in identifying patterns and spatial connections enables them to reveal critical insights from the inputs. This skill also includes the ability to recognize inverse relationships, thus boosting their effectiveness in tasks that require a deep understanding of the interactions among various elements of the sequential data. Typically, a pooling layer follows a convolution layer which helps in removing insignificant features from the most prominent one by reducing the dimensionality. Max-pooling is preferred to implement the DL network in this research which only selects the maximum values in the layer $\boldsymbol{x}_i^{(l+1)}$ and which can be represented as:

$$y_i^{(l+1)} = \max(x_i^{(l)}, x_{i+1}^{(l)}, x_{i+2}^{(l)}, \dots, x_{i+K-1}^{(l)})$$
 (13)

where K is the size of the pooling window. Finally, to map the target output with the derived feature from the overlying convolution layers, a Fully Connected (FC) dense layer is used. It can be mathematically represented as:

$$z_i^{(l+1)} = f(w_{ii}^{(l)} \cdot x_i^{(l)}) + b_i^{(l)}$$
(14)

where $z_i^{(l+1)}$ represents the i-th output in layer (l+1); $w_{ij}^{(l)}$ is the weight associated to connect j-th node in layer (l) $(x_j^{(l)})$ to the i-th output in layer (l+1); $b_i^{(l)}$ is the bias term to relate the i-th output in layer (l+1). We have

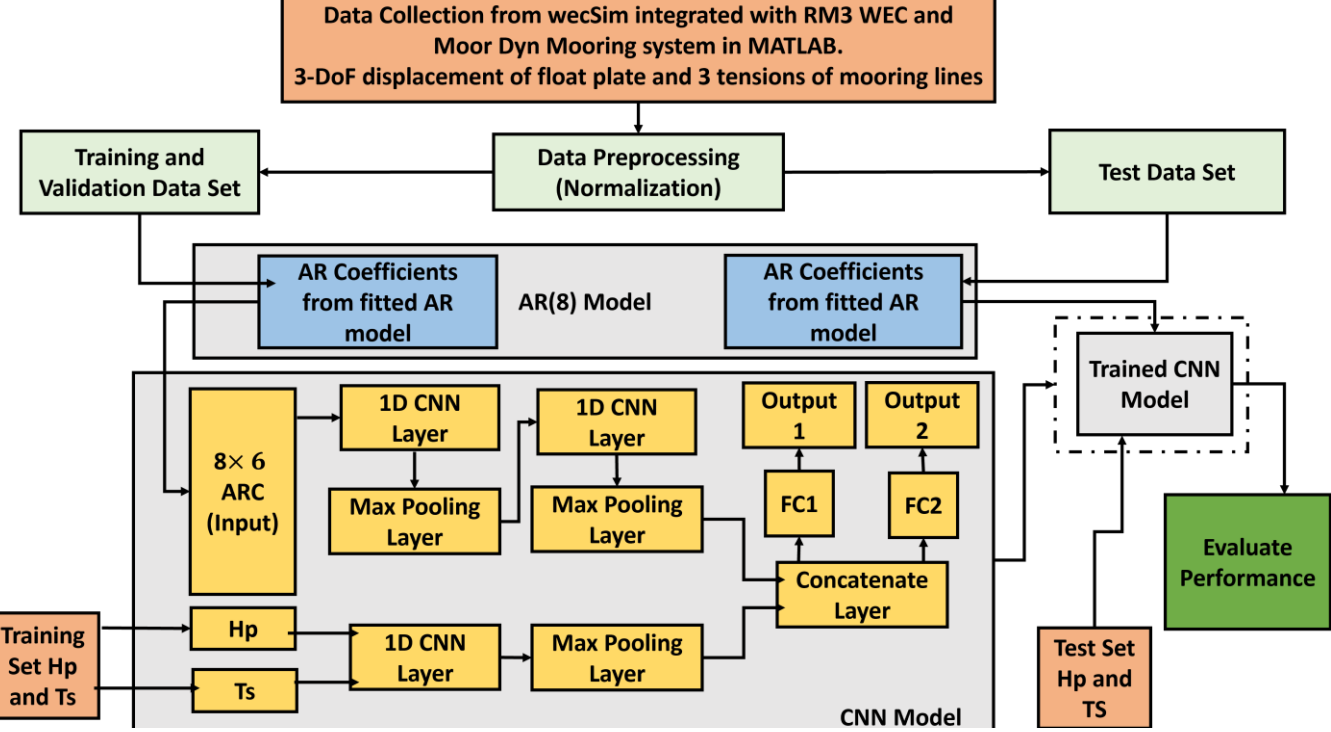


Fig 2: Overall System Framework

used Sigmoid activation function for the FC layer to enable continuous prediction of the outputs for a supervised regression problem. The sigmoid activation function can be represented as:

$$f(x) = \frac{1}{1 + e^{-x}} \tag{15}$$

To initiate the backpropagation algorithm and update the weights, we define the Mean Square Error (MSE) as the loss function which is a common practice for a regression problem. The MSE can be represented as:

$$MSE = \frac{1}{Nt} \sum_{i=1}^{Nt} (y_i - \hat{y}_i)^2$$
 (16)

where, Nt is the number of data points in the training sample set, y_i is the i-th target output and \hat{y}_i is the predicted value for the i-th data point. The gradient of the MSE loss is computed with respect to the output to start with as:

$$\frac{\partial MSE}{\partial \hat{y_i}} = 2 \frac{1}{Nt} (y_i - \hat{y}_i)$$
 (17)

The gradient of the loss w.r.t. a weight $(w_{ij}^{(l)})$ during the k-th epoch during training in the network is computed using the chain rule as:

$$g_{ij}^{(l)} = \frac{\partial MSE}{\partial \widehat{y_i}} \cdot \frac{\partial \widehat{y_i}}{\partial w_{ij}^{(l)}}$$
(18)

The update rule of the weights follows Adam optimization algorithm in this work which uses an adaptive learning rate approach by having personalized learning rates for each parameter [24].

D. The Fault Diagnosis Framework

The overall fault diagnosis framework is depicted in Fig. 2. As shown in the figure, dynamic responses of the RM3 WEC (including the motion responses and mooring tensions) are collected from the numerical simulation framework under varied fault and ocean conditions. More specifically, two

fault conditions are considered: (1) a reduction in stiffness by 0% to 10% due to corrosion, and (2) an increase in mass from 0% to 10% due to biofouling, in 1% increments. It is noted that in this research, we assume uniform degradation across all three mooring lines.

The collected data will then be normalized and separated into the training/validation set and the testing set. The training/validation data will be fitted with the AR model to identify the AR coefficients. These coefficients, along with the wave characteristics (significant wave height and peak period), will be used as the inputs of the CNN model, paired with the associated faults as outputs to train the CNN model. Once the model is trained, the performance of the CNN model will be validated with the testing data (never seen during training and validation) which are selected from the overall dataset with random fault and wave conditions.

III. RESULTS

Numerical simulation results are presented in this section. The WEC dynamic responses are analyzed first to understand their sensitivity to faults. Next, the identification of the AR model is shown. Finally, the training and testing of the CNN model for fault diagnosis are demonstrated.

A. WEC dynamic responses

The WEC dynamic responses are analyzed in this section. Fig. 3 shows nine dynamic responses generated from the developed simulation framework, which include 6-DoF motion responses as well as the mooring tensions under an irregular wave with a PM spectrum, a significant wave height of 4.33 m, and a peak period of 13.42 s. The signals generated from a healthy state are compared with those from a damaged state with a 10% increase in mass to analyze the impact of faults on the system responses. We can clearly tell from the figure that the RM3 WEC has dominant responses in surge, heave, and pitch, which are significantly impacted by the

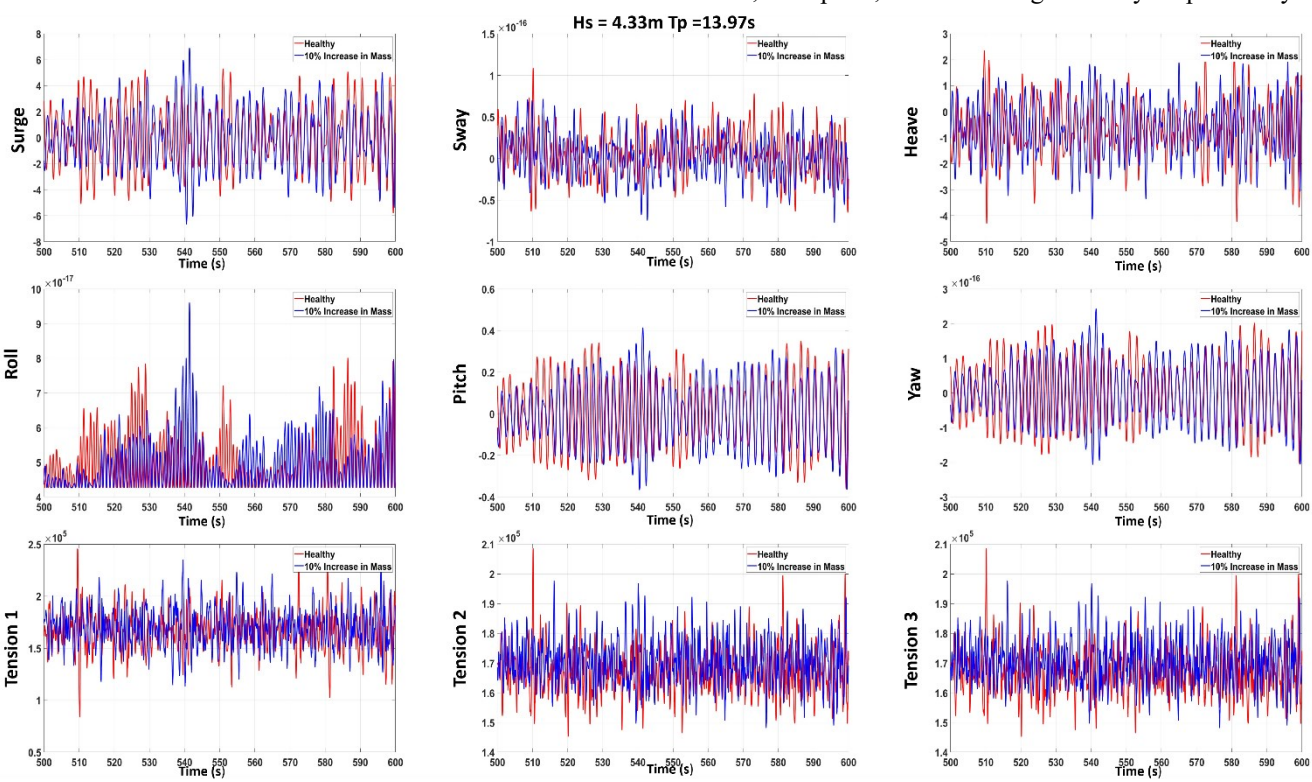


Fig 3: Comparison of the dynamic response of healthy mooring system with 10% increase in mass of mooring lines

faults, while the sway, roll, and yaw responses are negligible. Moreover, it is not surprising that the mooring tensions are significantly influenced by the faults since they directly reflect any changes in mooring structure integrity. In this context, it is reasonable to select surge, heave, pitch

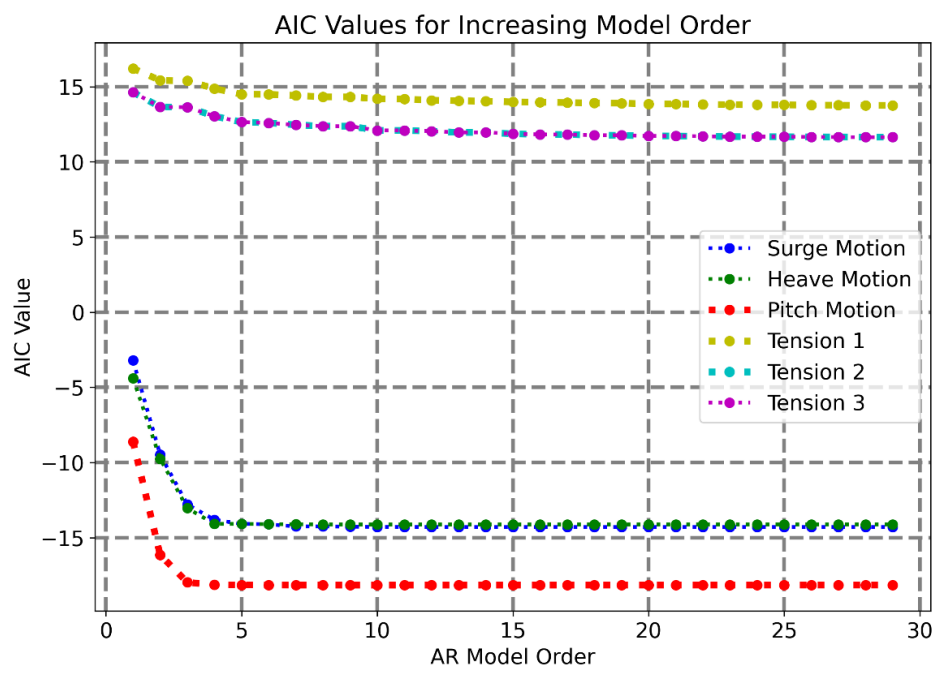


Fig 5: AIC evaluation with increasing model order for all the 6 dynamic responses

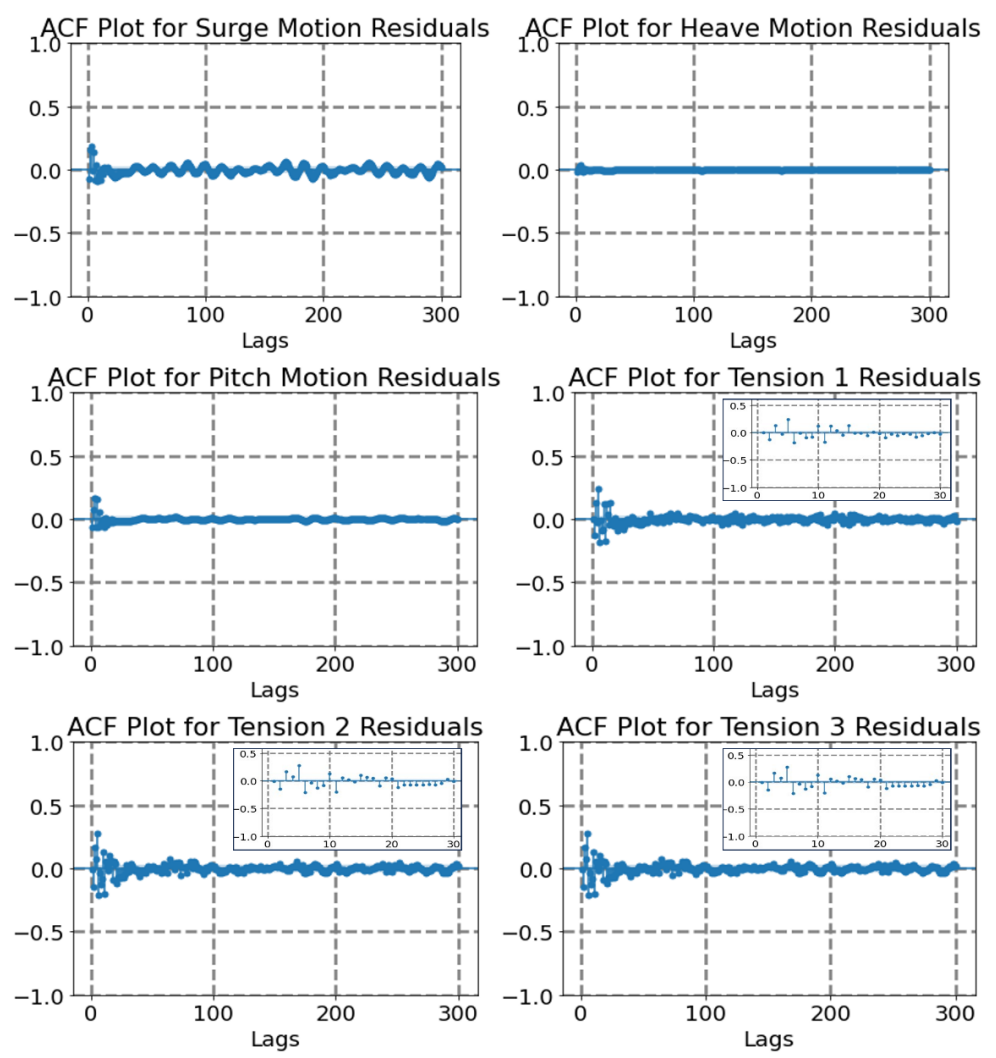


Fig 4: ACF plots of residuals for all the 6 dynamic response

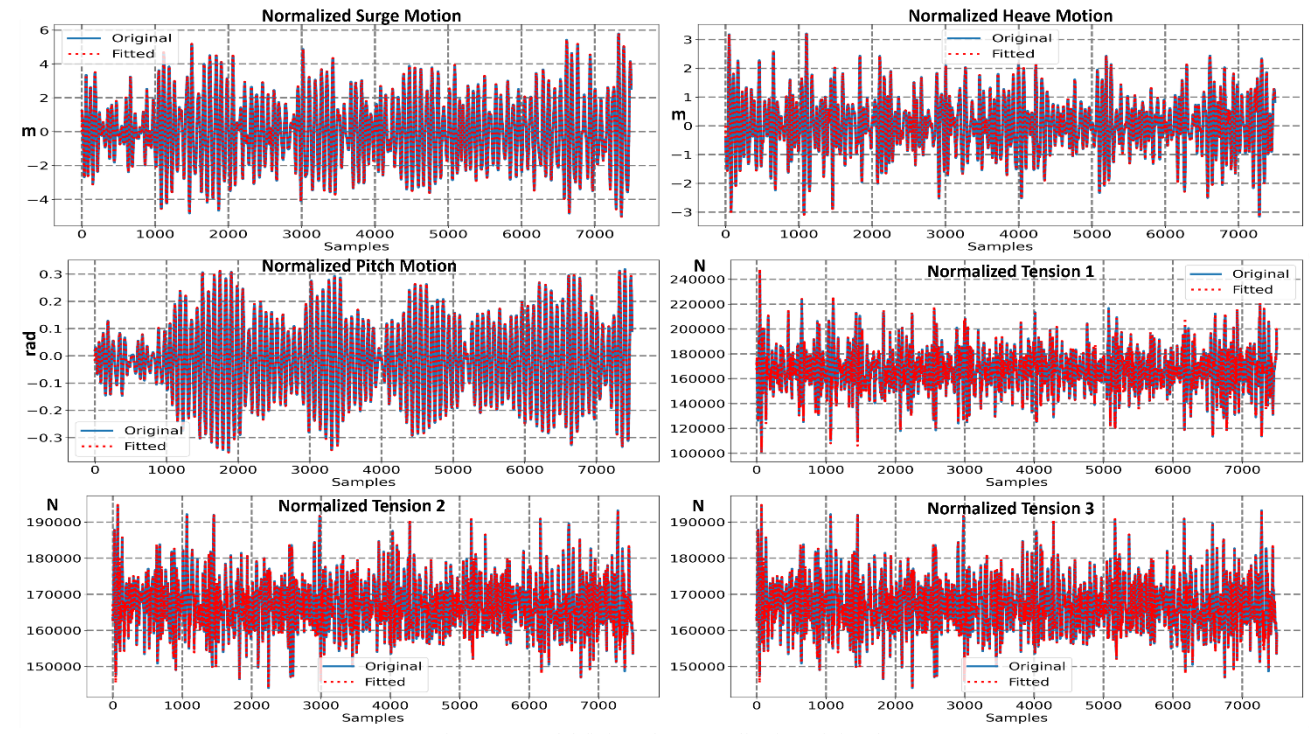


Fig 6: AR model fitting after normalization of signals

responses, and mooring tensions as the signal inputs for fault diagnosis.

B. AR model Identification

As introduced earlier, an AR model will next be identified for each of the system responses. The measurements collected under a healthy state with a significant wave height of 4.33m and a peak period of 13.42s are utilized as the baseline dataset to select the order of the AR model, which will then be used for the AR model for other signals. This standardization ensures a consistent model order across the dataset and allows for the formulation of AR coefficients for faulty measurements relative to the healthy state.

The selection of the AR model order primarily relies on the analysis of the AIC criterion (Eq. (10)). It is noted that this criterion combines the likelihood and the penalty of the model order, indicating that the user should select a model order such that the AIC is minimized (representing a small variance of the residuals) and the model order is relatively low (to save computational cost). Fig. 4 illustrates the AIC values for various system responses with an increasing model order. The figure shows the convergence of AIC values across all six dynamic responses, leading to the selection of a model order of P = 8.

After the AR model is identified, it is critical to inspect the AutoCorrelation Function (ACF) for the residuals between the actual and fitted signals, as presented in Fig. 5. It is clearly visible in the figure that the residuals of surge, heave, and pitch responses are well within the 95% confidence bound. Regarding the mooring tensions, a small number of lags (accounting for 3.3% to 5%) are outside the 95% confidence bounds. Overall, the signals predicted using the AR model with the identified model order have a good agreement with the actual data, which is presented in Fig. 6 (original data versus fitted for three motion responses and mooring tensions).

C. Training and testing of CNN model

As presented in Fig. 2, the CNN model accepts the AR coefficients as inputs. In addition, the wave characteristics, including the significant wave height and peak period, are also considered in the inputs to further address the challenge of fault diagnosis subject to ocean wave randomness. Accordingly, we will have two sets of inputs to the DL architecture: Input 1 will be an 8×6 array of AR coefficients, where 8 represents the AR model order (as identified in the last section) and 6 represents the 6 system responses; Input 2 will be a (2×1) array of [Hp, Ts].

In the design of the DL architecture, the first set of inputs is processed with two CNN layers and two MaxPooling layers. This is imperative as they contain temporal differences, which are essential for feature extraction. The second set of inputs helps the DL model determine the state of the ocean wave, which influences the dynamic responses. Therefore, the second set of inputs is processed with a single layer of CNN and a MaxPooling layer with a relatively smaller number of kernels. The final DL architecture is defined as follows:

Layer 1: Input1(8,6)

Layer 2: ID-CNN (ReLU, (3×1), 64 filters)

Layer 3: MaxPooling $(2 \times 1)(Layer2)$

Layer 4: 1D-CNN (ReLU, (3×1), 128 filters

Layer 5: MaxPooling (2×1)

Layer 6: Input2 (2,1)

Layer 7: 1D-CNN (ReLU, (3×1), 16 filters

Layer 8: MaxPooling (2×1)

Layer 9: Concatenate (Layer 5, Layer 8)

Layer 10: Dense (Sigmoid, (2×1))

Layer 1 to Layer 5 process the AR coefficients, and Layer 6 to Layer 8 process the ocean states. The nodes of Layer 5 and Layer 8 are flattened to form a 1D array before being concatenated in Layer 9. Thus, Layer 9 includes the contribution of the AR coefficients and the features extracted from the ocean states. Finally, the concatenated feature set from both inputs is fully connected to predict the two outputs: Stiffness Reduction and Accumulation of Mass. TensorFlow and Keras were used to implement the DL model.

To evaluate the performance of the trained DL model, common regression evaluation metrics such as Mean Square Error (MSE), Mean Absolute Error (MAE), and coefficient of determination (R²) are used:

$$MSE = \frac{1}{N} \sum_{i=1}^{N} (y_i - \hat{y}_i)^2$$
 (19a)

$$MAE = \frac{1}{N} \sum_{i=1}^{N} |y_i - \hat{y}_i|^2$$
 (19b)

$$R^{2} = 1 - \frac{\sum_{i=1}^{N} (y_{i} - \hat{y}_{i})^{2}}{\sum_{i=1}^{N} (y_{i} - \overline{y}_{i})^{2}}$$
(19c)

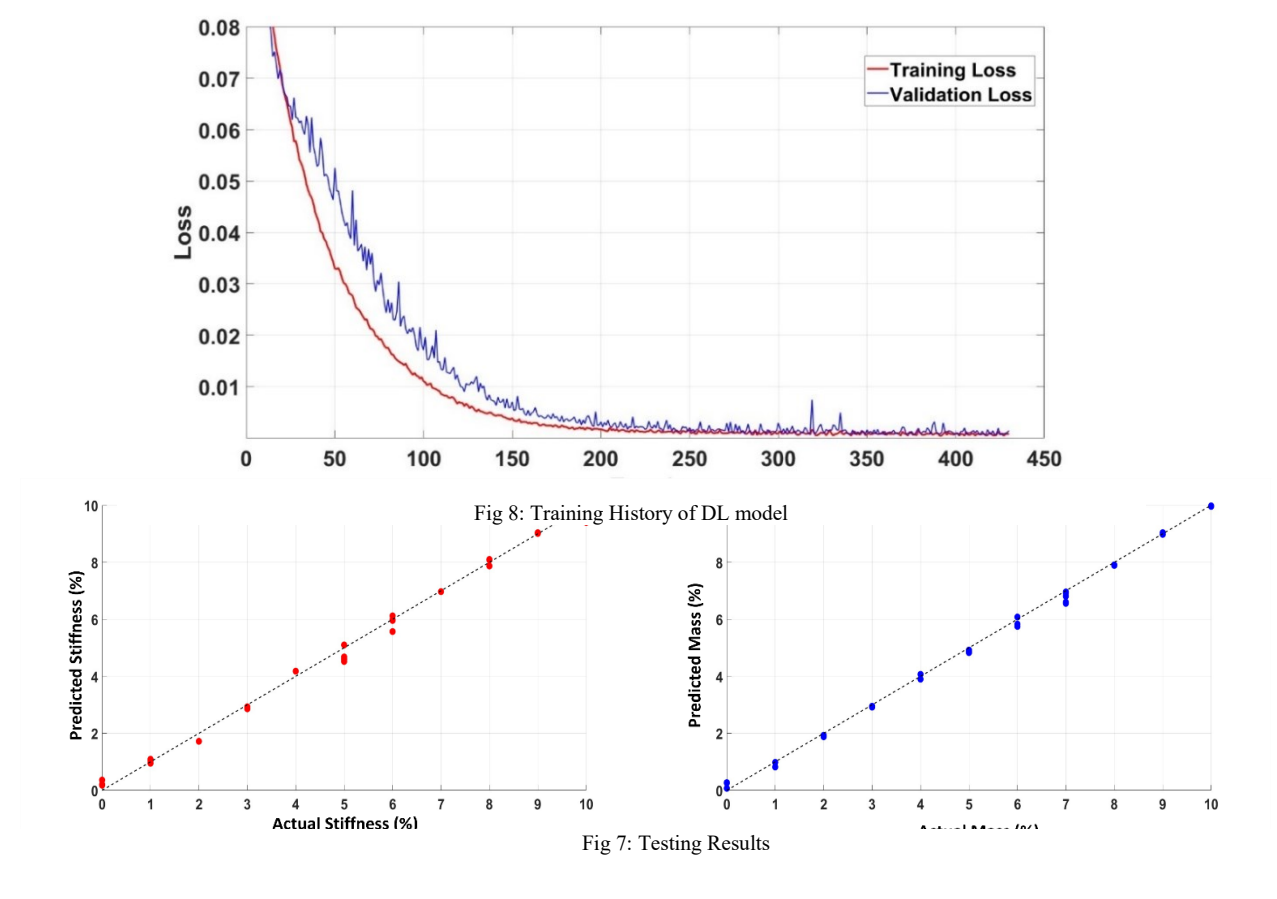
where N denotes the total number of sample, y_i represents the ground truth value, \hat{y}_i represents the predicted value and \overline{y}_i is the mean of the ground truth values.

Table 2: Wave Conditions

Wave Condition	Significant Wave Height (Hs) (m)	Peak Period (Tp) (s)
Wave Condition 1	1	8
Wave Condition 2	1.65	8.81
Wave Condition 3	4.33	13.97
Wave Condition 4	1.96	16.42
Wave Condition 5	2.19	11.92

Overall, 605 samples are collected from numerical simulations, accounting for 11 × 11 fault conditions for

reduced stiffness and increased mooring line mass, respectively. Moreover, 5 sea states are considered in the overall dataset, which are presented in Table 2. It is noted that wave conditions 2 to 5 are adopted from the representative real sea states of PacWave, Oregon [25]. Each data set is simulated by the developed model for 2000 seconds at a sampling rate of 40Hz. The first 500 seconds are discarded due to transient responses, and the remaining 1500 seconds are utilized for fault diagnosis and are downsampled to 5Hz. The overall dataset is then split into training and test set randomly. The test set here includes random coupling of the faults along with random ocean states presented in Table 2. The remaining samples are split into a training and validation set randomly with 80 validation samples. The training is set to be performed for 2000 epochs with an early stopping condition set on the validation losses. The learning rate for the model is defined as 1e⁻⁴ and the Adam optimization parameters $\beta 1$ is set to 0.9, $\beta 2$ is set to 0.999, decay is set to 0. The history of training and validation losses is presented in Fig. 7. The figure shows the training and validation loss continuously decreased during the training process. The model undergoes normal fitting without overfitting which is evident from the validation loss curve. The model stops training after 350 epochs due to the early stopping condition imposed on the model. The model took approximately 129.9 seconds to train 26,530 parameters for the DL model on a 64bit, 32GB and 2.1 Ghz hardware. At the end of training, the validation loss is slightly more than the training loss. Once the training is concluded the model is tested with the test sample which was randomly picked from the overall data set. It should be noted that the combination of faults and the ocean condition present in the test sample is never seen during the training or validation. Fig. 8 shows the test results where the predicted outputs are plotted against the ground



truth values for both the mooring faults. The figure clearly demonstrates that the DL model can predict the faults well. Table 3 shows the performance metrics evaluated during testing. The R² values yielded during testing for the prediction of both the mooring faults are close to 1 (0.994 for stiffness predictions and 0.997 for mass accumulation predictions) which serves as a strong validation of the proposed model. Moreover, it should be noted that the dataset collected was simulated using irregular ocean waves with random phase shifts. The coupling of AR coefficients and wave characteristics as the inputs for CNN evidently addresses the randomness introduced by ocean conditions.

Table 3: Test Results

rable 5. rest results			
Performance	Mooring Fault 1	Mooring Fault	
Metric	(Stiffness	2(Mass	
	Reduction)	Accumulation	
MSE	0.00059167633	0.00028773324	
MAE	0.01895002	0.013178647	
\mathbb{R}^2	0.9945779	0.996992	

IV. CONCLUSION

This study successfully demonstrates the capability of a combined AR and CNN framework to effectively diagnose faults in WEC mooring systems. By adapting machine learning algorithms to process and analyze AR coefficients derived from dynamic response data, we have established a robust system capable of accurately identifying damage under varying conditions. The AR model efficiently captures temporal features which are enhanced through CNN's spatial pattern recognition capabilities, providing a comprehensive tool for SHM. The simulations have validated the model's efficacy, with results showing high accuracy and the ability to handle real-world oceanic variabilities. Future work will aim to predict mooring system behavior under any ocean state. While the current study focuses on uniform degradation across three mooring lines, future research will aim to individualize the assessment for each mooring line. We also aim to improve robustness of the model to noises in the signal.

ACKNOWLEDGMENTS

Shangyan Zou and Abishek Subramanian are supported by NSF under grant CMMI - 2138522.

REFERENCES

- [1] Polinder, Henk, and Mattia Scuotto. "Wave energy converters and their impact on power systems." 2005 International conference on future power systems. IEEE, 2005
- [2] Clemente, Daniel, P. Rosa-Santos, and F. Taveira-Pinto. "On the potential synergies and applications of wave energy converters: A review." *Renewable and Sustainable Energy Reviews* 135 (2021): 110162.
- [3] Zhang, Yongxing, et al. "Ocean wave energy converters: Technical principle, device realization, and performance evaluation." *Renewable and Sustainable Energy Reviews* 141 (2021): 110764.
- [4] Hosseinzadeh, Shabnam, Amir Etemad-Shahidi, and Rodney A. Stewart. "Site selection of combined offshore wind and wave energy farms: a systematic review." *Energies* 16.4 (2023): 2074.

- [5] Xu, Sheng, Shan Wang, and C. Guedes Soares. "Review of mooring design for floating wave energy converters." *Renewable and Sustainable Energy Reviews* 111 (2019): 595-621.
- [6] Ma, Kai-tung, et al. "A historical review on integrity issues of permanent mooring systems." *Offshore technology conference*. OTC, 2013.
- [7] Kvitrud, Arne. "Lessons learned from Norwegian mooring line failures 2010–2013." *International Conference on Offshore Mechanics and Arctic Engineering*. Vol. 45424. American Society of Mechanical Engineers, 2014.
- [8] Angulo, Angela, et al. "Mooring integrity management: Novel approaches towards in situ monitoring." Structural Health Monitoring-Measurement Methods and Practical Applications (2017): 87-108.
- [9] Rémouit, Flore, et al. "Deployment and maintenance of wave energy converters at the lysekil research site: A comparative study on the use of divers and remotely-operated vehicles." *Journal of Marine Science and Engineering* 6.2 (2018): 39.
- [10] Eassom, Adrian, Kanishka Jayasinghe, and Clare Thomas. "Detection of Long-Term Changes in Mooring Stiffness Using Vessel Position Monitoring." International Conference on Offshore Mechanics and Arctic Engineering. Vol. 86830. American Society of Mechanical Engineers, 2023.
- [11] Yang, Shun-Han, et al. "Biofouling on mooring lines and power cables used in wave energy converter systems—Analysis of fatigue life and energy performance." *Applied Ocean Research* 65 (2017): 166-17
- [12] Liu, Yixuan, et al. "Physics-guided data-driven failure identification of underwater mooring systems in offshore infrastructures." *Health Monitoring of Structural and Biological Systems XVIII*. Vol. 12951. SPIE, 2024.
- [13] Sharma, Smriti, and Vincenzo Nava. "Condition monitoring of mooring systems for Floating Offshore Wind Turbines using Convolutional Neural Network framework coupled with Autoregressive coefficients." Ocean Engineering 302 (2024): 117650.
- [14] Cummins, W. E. "The impulse response function and ship motion." Report 1661, Department of the Navy, David W. Taylor Model Basin, Hydromechanics Laboratory, Research and Development Report, October 1962 (1962)
- [15] Raghavan, V., et al. "A comparative study on BEM solvers for Wave Energy Converters." Trends in Renewable Energies Offshore (2022): 441-447
- [16] Hall, Matthew, and Andrew Goupee. "Validation of a lumped-mass mooring line model with DeepCwind semisubmersible model test data." *Ocean Engineering* 104 (2015): 590-603.
- [17] Akaike, Hirotugu. "A new look at the statistical model identification." *IEEE transactions on automatic control* 19.6 (1974): 716-723.
- [18] Ljung, Lennart. "Theory for the user." *System identification* (1987).
- [19] Burg, John Parker. "A new analysis technique for time series data." Paper presented at NATO Advanced Study

- Institute on Signal Processing, Enschede, Netherlands, 1968 (1968).
- [20] Nair, K. Krishnan, Anne S. Kiremidjian, and Kincho H. Law. "Time series-based damage detection and localization algorithm with application to the ASCE benchmark structure." *Journal of Sound and Vibration* 291.1-2 (2006): 349-368.
- [21] Brockwell, Peter J., and Richard A. Davis. *Time series:* theory and methods. Springer science & business media, 1991.
- [22] Ige, Ayokunle Olalekan, and Malusi Sibiya. "State-of-the-art in 1D Convolutional Neural Networks: A Survey." *IEEE Access* (2024).
- [23] Nwankpa, Chigozie, et al. "Activation functions: Comparison of trends in practice and research for deep learning." *arXiv preprint arXiv:1811.03378* (2018).
- [24] Kingma, Diederik P., and Jimmy Ba. "Adam: A method for stochastic optimization." *arXiv* preprint *arXiv*:1412.6980 (2014).
- [25] Zou, Shangyan, et al. "Wave energy converter arrays: A methodology to assess performance considering the disturbed wave field." *Renewable Energy* (2024): 120719.